Journal of Solid State Electrochemistry
https://doi.org/10.1007/s10008-024-06169-x

ORIGINAL PAPER

Effect of titanium dioxide nanofillers on the properties of gel-polymer electrolytes and power conversion efficiency of dye-sensitized solar cells

R. P. Chandrika[1] · S. M. S. Gunathilaka[1] · J. P. Liyanage[1,2] · Kapila Wijayaratne[1,2] · G. R. A. Kumara[3] · N. G. A. Karunathilaka[4] · L. Ajith DeSilva[5] · T. M. W. J. Bandara[1,2]

Received: 5 October 2024 / Revised: 16 November 2024 / Accepted: 9 December 2024

Abstract
TiO_2 nanoparticles were gradually incorporated into a gel-polymer electrolyte to optimize the nanofiller composition to develop stable and highly efficient solid-state DSSCs. For this purpose, TiO_2 nanoparticles (13 nm) were amalgamated (0–25%) to the polyethylene oxide-based polyiodide gel-polymer electrolyte. The nanofiller-infused electrolytes were sandwiched within six-layer photoanodes sensitized with N719 dye and platinum electrodes to assemble DSSCs. The cell efficiency and electrolyte conductivity are highly dependent on the TiO_2 nanoparticle content. The electrolytic conductivity and DSSC efficiency are maximum at the optimal nanofiller percentage of 17.50%. Nanofiller-free control cell has an efficiency of 5.70%, while the optimally nanofiller-infused DSSC shows the highest efficiency of 7.30%, yielding a 28.1% efficiency improvement. This boost in efficiency resulted in enhanced conductivity, suppression of charge recombination due to the addition of smaller-sized nanoparticles, and the utilization of an appropriate photoanode. This study uncovers valuable insights into developing more efficient DSSCs by integrating nano-additives in the electrolyte.

Keywords Composite electrolyte · Gel-polymer electrolyte · Ionic conductivity · Nanofiller · Titanium dioxide nanoparticle · DSSC

Introduction

In recent years, solar cells have been a focal point in energy research due to their prospected potential as a sustainable, renewable, and low-maintenance energy source. Compared to most renewable energy technologies, photovoltaic technology stands out as a direct conversion method of solar energy to electrical energy. The frontrunner among photovoltaic technologies is the silicon solar cells, with efficiency being above 20% [1]. However, high production costs and complicated fabrication procedures are the main drawbacks of silicon-based solar cells [2]. DSSCs have attractive characteristics such as less complicated fabrication, high environmental compatibility and sustainability, low production cost, and high efficiency under low light conditions [3–5]. After the successful development of nanocrystalline TiO_2 thin film–based DSSCs by Grätzel [6], numerous efforts have been made to improve the photovoltaic performance of DSSCs. So far, more than 29,000 research publications have been published on DSSCs (Table 1). In general, DSSCs are composed of nanocrystalline TiO_2 photoanode to harvest the light energy, electrolyte-containing redox couple for the regeneration of the dye and electrolyte by itself during the operation, and Pt counter electrode to collect the electrons from the external circuit [7–9]. Among the components of the DSSCs, the electrolyte plays a major role in improving their efficiency and operational stability [9, 10]. Figure 1 shows the basic operational chemistry and

✉ T. M. W. J. Bandara
wijendra@sci.pdn.ac.lk; awijendr@yahoo.com

1 Postgraduate Institute of Science, University of Peradeniya, Peradeniya, Sri Lanka

2 Department of Physics, Faculty of Science, University of Peradeniya, Peradeniya, Sri Lanka

3 National Institute of Fundamental Studies, Hantana Road, Kandy 20000, Sri Lanka

4 Department of Mathematics, Faculty of Science, University of Kelaniya, Kelaniya, Sri Lanka

5 Department of Physics, University of West Georgia, Carrollton, USA

Published online: 17 December 2024

Table 1 The number of publications per year where titles, abstracts, or keywords contain "dye + sensitized + solar + cells + (polymer electrolyte/composite electrolyte/nanofillers/TiO_2 nanofillers)" (data retrieved from Scopus platform on 29 April 2024)

Year	Keyword				
	Dye + sensitized + solar + cells	Dye + sensitized + solar + cells + …			
		Polymer electrolyte	Composite electrolyte	Nanofillers	TiO_2 nanofillers
2024	454	18	15	3	2
2023	1140	50	39	6	0
2022	1273	70	47	3	0
2021	1402	73	34	6	3
2020	1551	82	37	1	0
2019	1692	89	32	8	2
2018	1847	103	47	5	0
2017	1927	102	39	1	0
2016	2152	109	60	2	0
2015	2304	117	52	1	0
2014	2772	115	69	4	1
2013	2296	107	60	2	1
2012	1933	81	33	0	0
2011	1729	101	37	1	0
2010	1285	90	30	3	1
2009	866	58	14	1	0
2008	649	57	13	2	2
2007	499	40	16	0	0
2006	429	38	12	0	0
2005	343	31	11	0	0
2004	241	21	5	0	0
2003	156	14	1	0	0
2002	137	14	5	0	0
2001	70	8	0	0	0
2000	59	0		0	0
From 2000 to 1978	123	1	0	0	0
Total	29,329	1589	708	49	12

charge transport in dye or quantum dot–sensitized solar cells, as described in the following 8 steps: 1. Light absorption: A dye or quantum dot sensitizer, which is bound to the nanoporous TiO_2 photoanode, absorbs photons from sunlight. 2. Electron excitation: Electrons in the ground state (HOMO) of the dye molecule or quantum dot are promoted to the excited state (LUMO) after absorbing photons from light ($2D_{(HOMO)} + 2h\nu \rightarrow 2D^*_{(LUMO)}$). 3. Excited electron injection: The excited electron from the dye molecules is injected into the conduction band of the photoanode semiconductor (TiO_2), leaving the dye molecules in an oxidized state. This electron injection contributes to efficient charge separation. 4. Electron transport through a semiconductor (TiO_2): The injected electron travels through the semiconductor to the conductive photoanode substrate (FTO) by diffusion. 5. Electron flow in an external circuit: Electrons reach the photoanode substrate and flow through an external circuit, generating an electric current that can power a load before returning to the cathode (counter electrode). 6. Electron transport through the cathode: Electrons coming from the external circuit travel to the cathode-electrolyte interface through the platinum or graphene counter electrode. 7. Reduction at the cathode: At the cathode, electrons that passed through the external circuit reduce the electrolyte's oxidized species (I_3^-) to its reduced form (I^-), completing the redox cycle ($I_3^- + 2e^- \rightarrow 3I^-$). 8. Regeneration of dye and cycle repeat: The oxidized dye/quantum dot is regenerated by receiving an electron from the electrolyte redox couple (I^-/I_3^-) in DSSCs ($3I^- + 2D^+ \rightarrow I_3^- + 2D$). This step restores the dye molecule to its ground state. The regenerated dye/quantum dot prepares the cell for the next cycle of light absorption, charge separation, and current generation. 9. Undesired recombination of dye. These steps contribute to converting light energy into electrical energy in DSSCs and

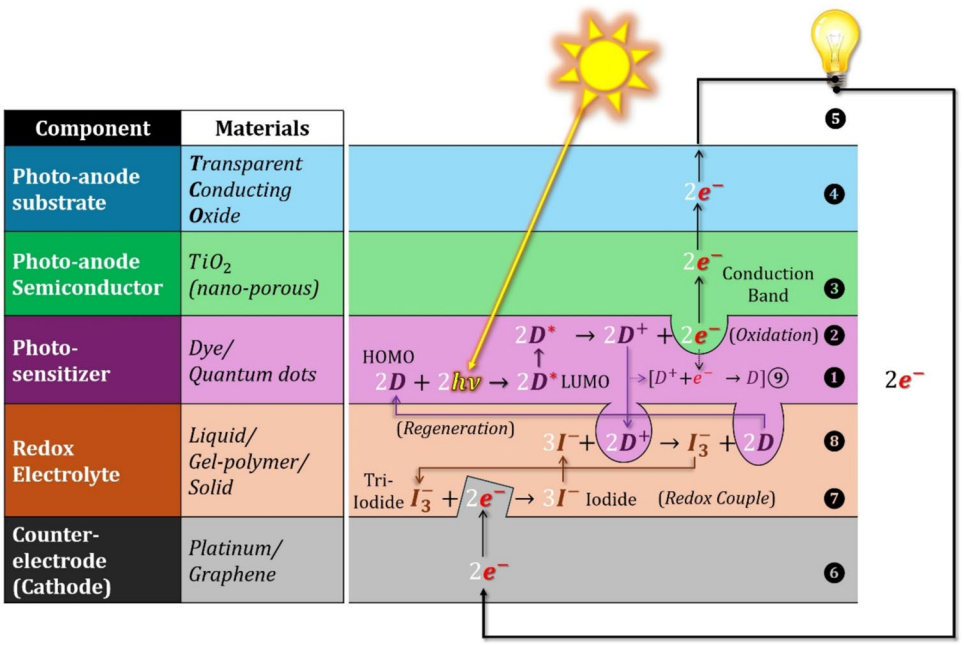

Fig. 1 The chemistry and charge transport of a dye or quantum dot–sensitized solar cell

QDSSCs by maintaining efficient transport within the cell. Among the components of the DSSCs, electrolytes play a significant role in improving their efficiency and operational stability [7].

The electrolyte governs the transfer and transport of charge carriers between two electrodes and continuously regenerates both dye and electrolyte itself during the operation of DSSCs [9]. Electrolytes suitable for high-performing DSSCs should have specific physical and chemical characteristics. The electrolyte should ensure the rapid diffusion of charge carriers between two electrodes; in other words, high ionic conductivity of respective redox species is needed. This causes the electrolyte and dye molecules to regenerate rapidly by themselves and maintains the high interfacial contact between the photoanode and cathode. The electrolyte should be highly stable during the operation of DSSCs. The presence of volatile, degrading, and reactive components in the electrolyte devastates the long-term stability of the cells [11]. It should also be chemically compatible with the other components (electrolyte species should not corrode electrodes) in the cells while having low cost, non-flammability, and low toxicity. In particular, the liquid electrolyte–based cells should be properly sealed to prevent possible leakages and component evaporation [9, 12, 13]. According to the latest reports, the maximum photoconversion efficiency of DSSCs has reached 15.0%; however, such high-performing cells contain problematic liquid electrolytes [14, 15].

Researchers have attempted to develop DSSC by replacing liquid electrolytes with gel or solid polymer electrolytes since they offer several advantages such as high stability, ease of sealing, and advanced flexibility of structure design [16, 17]. Gel or solid polymer electrolytes provide higher stability by limiting leakage and evaporation of components in electrolytes [18, 19]. Solid or gel electrolytes are less flammable, safer to handle, and less prone to accidents. The use of solid or gel electrolytes can simplify the sealing process of the DSSC, making it more cost-effective and potable. Using flexible solid/gel-polymer electrolytes and flexible and lightweight DSSC devices can be developed.

Table 1 gives an overview of the research trends in the field of dye-sensitized solar cells and the use of polymer electrolytes over the past few decades based on the Scopus database (as of 29 April 2024). Over 29,000 research publications containing the words "dye," "sensitized," "solar," and "cell" in their title, abstract, or keywords have been published. According to Scopus, about 1589 research articles relate to gel-polymer electrolyte–based DSSCs. However, this survey reveals only as few as 49 publications related to nanofiller-added solar cells have been published from 1978 to April 2000. Out of those, only 12 are associated with TiO_2 nanofiller–based solar cells, which makes this study essential to the photovoltaics research community.

Nanotechnology to develop DSSCs

Nanotechnology has been successfully applied to enhance the overall efficiency and stability of the DSSCs via nano-modified electrolytes and photoanodes [20, 21]. In particular, nanoscale additives such as nanofillers (NFs) can improve ionic conductivity in solid/gel-polymer electrolytes. Such electrolytes are named nanocomposite electrolytes, and NFs in such electrolytes contribute to enhancing ionic conductivity and other properties like mechanical strength. The application of such electrolytes enhances stability,

minimizes internal resistance, and ensures an efficient charge transfer process within the solar cells. Because of the high surface area of such nanomaterials, nanofiller-added electrolytes provide ample free space for ion diffusion and charge transport [22, 23]. Nano-additives can enhance the interface between the electrolyte and the rest of the cell components (photoanode, photosensitive dye, and counter electrode), reducing the recombination losses and improving the charge collection and transportation [12]. Incorporation of nanoparticles into electrolytes would also prevent the aggregation of redox species, resulting in uniform charge distribution and showing stable performance of DSSCs. The use of smaller fillers is more advantageous since their surface area-to-volume ratio is higher. Therefore, the incorporation of smaller nanoparticles into electrolytes enhances the overall stability and longevity of the DSSCs.

TiO_2 nanofillers

Nanoscale inorganic materials or nanofillers (NFs) can be added to DSSC electrolytes to optimize performance. Such NFs are derived from metal oxides, metal sulfides, and carbonaceous materials. These nanoparticles should have a smaller particle size than the pore size of the TiO_2 film of the electrode. As metal oxide material, SiO_2, Al_2O_3, and TiO_2 nanoparticles are being used in preparing nanocomposite electrolytes [10, 24, 25]. Among these, TiO_2 metal oxide nanoparticles have attracted significant attention due to their unique and desirable characteristics along with the ease of synthesis. TiO_2 is an inexpensive, non-toxic, and naturally occurring material. There are three different crystal phases of TiO_2, namely, rutile, anatase, and brookite. The structure of rutile and anatase is tetragonal, whereas the structure of brookite is orthorhombic [26–28]. Various forms of TiO_2 nanoparticles, including nanotubes, nanospheres, and nanorods, are used as NFs for the development of polymer electrolytes for secondary batteries. High surface area, nano-porosity, optical transparency, chemical stability, substantial charge collection, high electron mobility, and wide band gap of TiO_2 improve the charge transport between two electrodes, reducing the energy losses of electron–hole recombination and enhancing the light absorption. Because of that, TiO_2 nanoparticle–incorporated electrolytes are highly effective in the performance enhancement of the DSSCs.

Several studies have demonstrated that incorporating materials such as SiO_2 and Al_2O_3 can create high-conductivity pathways for ionic motion at the filler electrolyte interface through Lewis acid–base interactions. As a result, the addition of these fillers significantly improves the overall ionic conductivity. The smaller-size TiO_2 particles (13 nm) are selected to be used in this study since smaller nanoparticles have a higher surface area-to-volume ratio, providing more active sites for interaction within the electrolyte. This contributes to enhancing the overall ionic conductivity of the electrolyte, which is a key factor in improving DSSC efficiency. Additionally, larger nanoparticles have a greater tendency to agglomerate, which can disrupt the homogeneity of the electrolyte and reduce ionic mobility.

Research study and background

This study provides vital insight into systematically incorporating TiO_2 nanoparticles into the gel-polymer electrolyte for DSSCs, with an emphasis on adjusting the nanoparticle percentage to determine the optimal concentration for maximum efficiency. By carefully regulating the TiO_2 nanoparticle content, this research aims to clarify the effect of these nanoscale additives on the overall performance of DSSCs. Power conversion efficiency and stability of the DSSCs are highly dependent on the properties of the electrolyte. A stable electrolyte prevents the corrosion of the electrodes and desorption of dye molecules from the semiconductor materials and aids the longevity of the solar cells. Efficient electron transport maintains the continuous flow of charges and minimizes the recombination, ensuring optimal power output from the cell. TiO_2 NFs enhanced the long-term stability, lowered the recombination losses, and improved the electron transport properties in order to satisfy the specifications for stable and efficient electrolytes for DSSCs, resulting in more effective and efficient solar energy devices.

According to the literature, only a few research papers (12) have been published on DSSCs developed using TiO_2 nanofiller–added gel-polymer electrolyte as in Table 1, citing the Scopus database. A summary including filler size, host polymer, and reported efficiency is tabulated in Table 2. The maximum efficiency reported for a nanofiller-added gel electrolyte–based solar cell is 9.09%. This has been obtained with 21 nm filler particles and poly(acrylonitrile-co-vinyl acetate) polymer along with acetonitrile as the solvent, which is volatile and toxic. In contrast, the presented study used 13 nm TiO_2 nanofillers integrated into a non-volatile and non-toxic PEO host polymer-based gel electrolyte. This study reports the highest efficiency obtained using non-volatile and non-toxic gel electrolytes.

Materials and methods

Preparation of the photoanodes

The DSSCs under study were prepared using highly porous TiO_2 multi-layer photo anodes that had been sensitized with a commercial ruthenium-based dye (N719). The multi-layer photoanodes were made by TiO_2 nanoparticle coating on the substrate of fluorine-doped tin oxide glass (FTO).

Table 2 Summary of the publications related to DSSC with TiO_2 nanofiller–based electrolytes

Publication year	Numbers of publications	Nanofiller size	Type of polymer	Efficiency (%)	Reference
2024	1	21 nm	Polyethylene oxide (PEO)	4.04	[29]
2021	3	13 nm	Poly(ethylene oxide) (PEO)	4.41	[30]
		240 ~ 250 nm	Polyethylene glycol (PEG)	6.10	[31]
		< 25 nm	Poly(ethylene oxide) (PEO)	5.02	[32]
2019	2	25–30 nm	Poly(vinylidene difluoride-co-hexafluoropropylene) (PVDFHFP)	5.93	[33]
		21 nm	Poly(acrylonitrile-co-vinyl acetate)	*9.09	[34]
			NA, *liquid electrolyte only*	#9.55	[34]
2014	1	21 nm	Polyethylene oxide (PEO)	4.12	[35]
2013	1	20 nm	Poly(ethylene oxide) (PEO)	2.87	[36]
2010	1	13 nm	Poly(epichlorohydrin)	3.90	[37]
2008	2	13 nm	Poly(vinylidene fluoride)	0.46	[38]
		22 nm	Polyethylene oxide (PEO)	7.19	[39]

During the preparation of the first layer of the photoanode, a slurry of TiO_2 nanoparticles with an average particle size of 13 nm (Evonik AEROXIDE® TiO_2 P 90) was spin-coated for 2 min at 2300 rpm on cleaned FTO glass substrates with sheet resistance 10 $\Omega\,cm^{-2}$. The TiO_2 slurry was prepared by mixing 0.5 g of TiO_2 with 2 ml of 0.1 M HNO_3, and the coated photoanodes were left to air-dry for approximately 5 h and were sintered at 450 °C for 30 min. The same process was carried out during the preparation of the second layer. In order to prepare the third layer, 0.5 g of TiO_2 nanoparticles with an average particle size of 21 nm (Evonik AEROXIDE® TiO_2 P 25) was mixed with 2 ml of 0.1 M HNO_3. The resulting TiO_2 dispersion was spin-coated for 2 min at 1000 rpm prior to annealing at 450 °C. The same procedure was followed to coat the fourth, fifth, and sixth layers. Previously optimized procedures and composition were used to prepare these photoanodes [40–42, 49].

Prepared multi-layer photoanodes were then sensitized by dipping in a 0.5 mM dye solution of N719 (Solaronix® SA) in ethanol for 24 h. Prior to the assembly of DSSCs, photoanodes were removed from the dye solution and washed with ethanol to remove any particulates and dye molecules that were loosely attached to the FTO. The gel-polymer electrolytes were sandwiched between the photo-sensitized multi-layer anodes and the platinum (Pt) counter electrodes to assemble DSSCs.

Preparation of the electrolyte

All chemicals used for preparation were sourced from Sigma-Aldrich®, having purity levels above 99%. LiI and Tetrahexyl-ammonium iodide (Hex_4NI) were vacuum-dried for 2 h at ~ 50 °C prior to the use. The carefully measured compounds, ethylene carbonate (EC) and propylene carbonate (PC), 4-tert-butyl pyridine (4TBP), 1-methyl-3-propylimidazolium iodide (MPII), (Hex_4NI), and LiI were combined in a closed vial in the proper order [42]. The resulting mixture was heated at 100 ℃ and was slowly added to polyethylene oxide (PEO). After completely dissolving the PEO, the mixture was allowed to cool to 40 ℃, and iodine (I_2) was added while stirring continuously. For the electrolyte, the stoichiometric formula is PEO(10)EC(40)PC(40)MPII(0.25)4TBP(0.85)Hex4NI(0.8)LiI(1.2)I_2(0.2), as per the previously optimized procedure [42, 43]. In order to prepare the TiO_2 nanoparticle–infused electrolyte, PEO relevant amount of TiO_2 nanoparticles was added with an average particle size of 13 nm at 0.0 to 25.0 wt.%. Before analyzing the gel-polymer electrolyte, it was kept at room temperature for 48 h. The weight and weight percentage of the constituent of each sample are tabulated in Table 3. Figure 2 shows the photographic images of inverted

Table 3 The percentage of TiO_2 NF, TiO_2 NF, and PEO weights for electrolyte samples

Electrolyte	TiO_2 (wt.%)	TiO_2 (mg)	PEO (mg)
Sample A	0.00	0.00	50.00
Sample B	2.50	1.25	48.75
Sample C	5.00	2.50	47.50
Sample D	7.50	3.75	46.25
Sample E	10.00	5.00	45.00
Sample F	12.50	6.25	43.75
Sample G	15.00	7.50	42.50
Sample H	17.50	8.75	41.25
Sample I	20.00	10.00	40.00
Sample J	22.50	11.25	38.75
Sample K	25.00	12.50	37.50

Fig. 2 The gel-polymer electrolyte series varying added TiO_2 percentage from 0.0–25.0%

bottles containing the prepared gel-polymer electrolyte series by varying the TiO_2 content.

Characterization

After preparing the DSSCs, characteristic parameters of DSSCs were obtained using a PEC-LO1 solar simulator under AM1.5 (1000 W m^{-2}) radiation conditions with the support of a potentiostat (Peccell® Technologies) device. The active cell area was 0.19 cm^{-2}. Data for current versus voltage were obtained under continuous irradiation.

To examine the electrochemical resistance of the electrolyte series and DC polarization, a Metrohm® Autolab PGSTAT128N instrument was used within the frequency range 0.1 Hz to 1.0 MHz at different temperatures from 20 to 80 ℃. There, the nanoparticle-incorporated gel-polymer electrolyte samples of 1 mm thickness and 9 mm diameter were sandwiched between two stainless steel electrodes.

To examine the FTIR spectra and morphology of the gel-polymer electrolyte, a Fourier transform infrared (FTIR) spectroscopy (FT/IR-6700 Spectrometer from JASCO®) and ZEISS® AXIO Lab.A1 Polarizing Laboratory Microscope by Primotech® were used. To study the light absorption of the electrolyte series, a UV–visible spectrophotometer (UV-1800 Shimadzu) was used.

To determine the layer thickness and examine the surface morphology of the 6-layer photoanode, a Zeiss Evo LS15 scanning electron microscope was used to obtain cross-sectional and surface SEM images.

Results and discussion

Complex impedance analysis

DC conductivity

The Nyquist plots of the TiO_2 NF-incorporated electrolyte series obtained at various temperatures are shown in Fig. 3a. As an example, the Nyquist plots of the high-conducting electrolyte (sample H) taken at different temperatures ranging from 20 to 80 ℃ are shown in Fig. 3a. Every other sample (A to K) also exhibits similar curves. Table 4 displays the ionic conductivity values of the NF-incorporated electrolyte series.

The DC resistance values of the electrolyte were derived by using the Nyquist plots to calculate the ionic conductivity of the electrolyte series. The conductivity values for these NF-incorporated electrolyte samples usually show enhanced conductivity at high temperatures due to the mobility enhancement of ions at elevated temperatures. Those DC resistances of electrolytes obtained were used to determine the ionic conductivity of the NF-infused electrolyte series, as depicted in Fig. 3b.

The conductivity variation of the electrolyte series upon TiO_2 composition at different temperatures is shown in Fig. 3b. The ionic conductivity of nanoparticle-incorporated electrolytes enhanced with the increase of TiO_2 nanoparticle percentage up to 17.5%. In this sample,

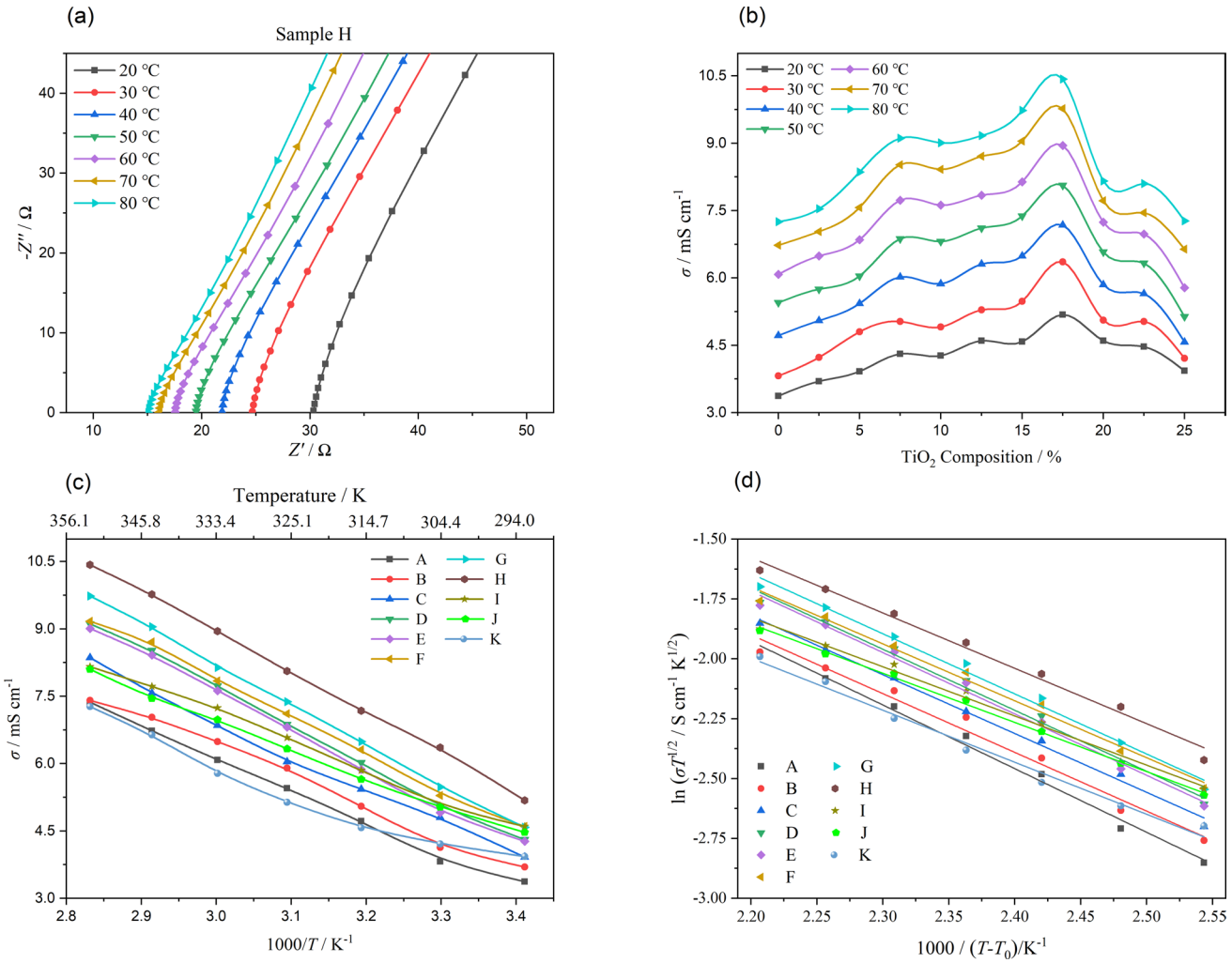

Fig. 3 **a** Nyquist plots for electrolyte sample H (containing 17.5 wt.% TiO_2 nanoparticles) taken at various temperatures, **b** conductivity variation with TiO_2 compositions of the electrolyte samples at different temperatures, **c** conductivity Arrhenius plots of the electrolytes series, and **d** Vogel-Tammann-Fulcher (VTF) plots of the electrolyte series

Table 4 Conductivity value for all electrolyte series with TiO_2 NFs added with various temperatures

Temperature (T)		Conductivity (σ/mS cm^{-1})										
T (℃)	T (K)	TiO_2 NFs added gel-polymer electrolyte sample										
		A	B	C	D	E	F	G	H	I	J	K
20	293.15	3.34	3.70	3.92	4.31	4.27	4.60	4.58	5.18	4.60	4.47	3.93
30	303.15	3.82	4.13	4.80	5.03	4.91	5.29	5.48	6.36	5.06	5.03	4.21
40	313.15	4.72	5.05	5.42	6.02	5.87	6.31	6.49	7.18	5.85	5.65	4.57
50	323.15	5.45	5.90	6.04	6.87	6.81	7.11	7.38	8.06	6.58	6.33	5.14
60	333.15	6.08	6.49	6.85	7.73	7.62	7.84	8.14	8.95	7.24	6.98	5.78
70	343.15	6.73	7.03	7.57	8.52	8.42	8.71	9.05	9.77	7.72	7.45	6.64
80	353.15	7.37	7.41	8.36	9.11	9.01	9.17	9.73	10.43	8.15	8.10	7.27

the conductivity of 5.18 mS cm^{-1} at 20 ℃ enhanced to 10.43 mS cm^{-1} when the temperature raised to 80 ℃. The increased amount (up to 17.5%) of TiO_2 NFs causes the separation of polymer chains in the PEO network and re-arranges them in a three-dimensional network, creating more free space. The free spaces act as additional

pathways for the migration of the I^-/I^-_3 ions through the electrolyte. TiO_2 NFs contribute to this process by inducing electrostatic interactions/Lewis acid–base interactions between O atoms of the PEO and hydroxyl group of the TiO_2 particles [8, 12]. These Lewis acid–base type interactions stabilize TiO_2 NFs on the surface of the PEO and prevent the recrystallization of polymer chains. Additional TiO_2 NFs contribute to the improvement of the ionic conductivity of the electrolyte by changing the morphology of the polymer network. As the TiO_2 particle concentration in the electrolyte increases further (above 17.5%), immobilized long polymer chains and NF aggregates will be formed, decreasing the conductivity of the electrolyte within the selected temperature range (from 20 to 80 ℃). This effect is known as the blocking effect of nanofillers or geometrical constrictions [8, 12, 44–46].

Temperature dependence of the ionic conductivity

Temperature dependence of ionic conductivity demonstrated non-Arrhenius behavior for all electrolyte samples in the series. The ionic conductivity of nanoparticle-incorporated electrolyte increases with the increase of TiO_2 nanoparticle percentage. As shown in Fig. 3c, the maximum conductivity is shown by the electrolyte sample H, which has 17.5 wt.% TiO_2. The low-temperature (20 ℃) conductivity of this electrolyte sample was 5.18 mS cm^{-1}, and a high-temperature conductivity of 10.43 mS cm^{-1} was shown at 80 ℃. It was also observed that the conductivities of all TiO_2 nanocomposite electrolytes in the examined temperature range (from 20 to 80 ℃) are closer to each other. In general, the observed conductivity value of all the investigated electrolyte samples was significant enough to fabricate high-performance nanocomposite gel-polymer electrolyte DSSCs.

Since the temperature dependence of conductivity was non-Arrhenius, the conductivity values were fitted using the Vogel-Tammann-Fulcher (VTF) model as in Eq. 1. The corresponding VTF plots are shown in Fig. 3d, and it demonstrates the validity of VTF behavior in temperature dependence conductivity [46]. In this model fitting, the glass transition temperature (T_0) of the samples was considered as − 100 ℃, and the appropriate selection is reflected by the better fitting shown in Fig. 3d. There, $\ln(\sigma T^{1/2})$ was plotted against $1000/(T-T_0)$, and the behavior of the electrolytes at various temperatures was examined using individual VTF plots. The fitted data confirms a linear trend. Furthermore, the pseudo activation energy and pre-exponential factors were calculated by fitting the data to the VTF equation and are included in Table 5. The free exponential factor, which is a measure of free ion concentration, fluctuates between 2.6 and 3.9 S cm^{-1} $K^{1/2}$. This variation can be attributed to the synergistic effects of the ion dilution effect and ion association/dissociation, driven by the escalating mass fraction of TiO_2. Samples A to H exhibit relatively higher pre-exponential factors, indicating a greater concentration of free ions, which contribute to higher conductivity. In contrast, samples I, J, and K show lower pre-exponential factors, suggesting reduced conductivity due to a lower concentration of mobile ions. This reduced conductivity can be attributed to the fact that, in these samples, only the loosely bound ions are mobile, while the tightly bound ions remain immobile. As a result over mobile ion concentration, the overall ionic conductivity is limited. This is further reflected in the lower activation energy for these samples, as only the loosely bound ions contribute to conduction, requiring less energy to become mobile. The observed decreasing E_a (drop in the activation energy) with the increasing TiO_2 content underscores the nanofiller's role in enhancing conductivity. The increase in conductivity of the electrolyte samples upon temperature increase can be attributed to the enhancement of mobility of ions at elevated temperatures resulting in decreased activation energy [47, 48].

Table 5 The pre-exponential factor, A, and activation energy, E_a, for all electrolyte series with varying TiO_2 NF percentages from 0.0 to 25.0%

Sample	A (S cm^{-1} $K^{1/2}$)	E_a (eV)
A	3.9	2.6
B	3.6	2.5
C	3.6	2.5
D	3.9	2.5
E	3.9	2.5
F	3.6	2.4
G	3.8	2.4
H	3.6	2.3
I	2.6	2.0
J	2.6	2.0
K	2.7	2.1

$$\sigma(T) = AT^{-\frac{1}{2}}\exp\left[\frac{-Ea}{K_b(T-T_0)}\right] \quad (1)$$

Complex AC conductivity

Generally, the complex conductivity of an electrolyte depends on the different kinds of polarization, such as dipole polarization, ionic polarization, electronic polarization, and the polarization of the electrodes [49]. Furthermore, the ionic conduction and dielectric behavior of the electrolytes get modified by the dynamics of charge species along with dipole and dielectric relaxation [46, 50]. Because of this complexity, the electrolyte examined in this study is expected to experience a variety of polarization mechanisms. Because of that, the real part (σ') and imaginary part (σ'') of the AC conductivity of electrolyte series with NFs are

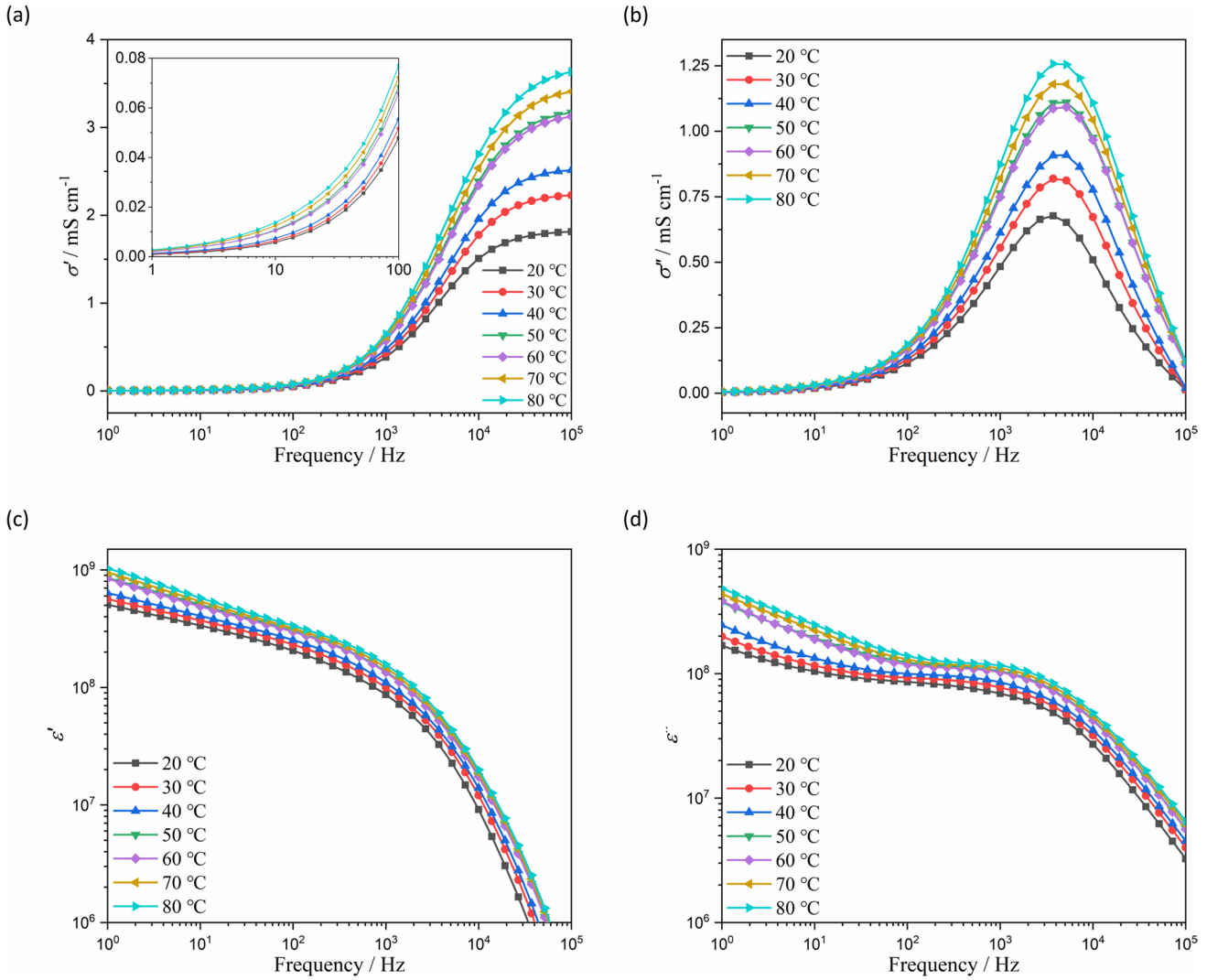

Fig. 4 Frequency dependence of **a** the real part of the AC conductivity (σ') (inset shows the low frequencies values), **b** the imaginary part of the AC conductivity (σ''), **c** the real part of the dielectric constant (ε'), and **d** the imaginary part of the dielectric constant (ε'') of the electrolyte sample H (that contains 17.5 wt.% TiO_2 NFs) at various temperatures

studied as a function of frequency at different temperatures from 20 to 80 ℃.

The variation of the frequency-dependent real part of the AC conductivity of sample H (with 17.5 wt.% TiO_2 NFs) is shown in Fig. 4a for several temperatures. All other samples (A to K) exhibited a similar trend. The real part of the AC conductivity increases with the increase in frequency due to the enhanced frequency-dependent polarization dynamics.

The AC conductivity reaches the DC limit at high frequencies, and these high-frequency values are similar to the DC conductivity values obtained via Nyquist plots as in Fig. 3a. All the conductivity curves for the electrolyte series tend to plateau at high frequencies as well as low frequencies. AC conductivity for the samples onsets a high-frequency plateau at 10^5 Hz as tabulated in Table 6. Also, due to the mobility enhancement of ions at elevated temperatures, these high-frequency plateau values increase with temperature for all electrolyte samples in the series.

As seen by Fig. 4a and its inset for representative sample H, the real part of the AC conductivity (σ') exponentially drops while approaching low frequencies (100 to 1 Hz). All other samples (A to K) exhibit similar behavior as well. This exponential drop can be traced to the relaxation of electrode polarization. At low frequencies, there are fewer mobile ions in the bulk due to the increased charge build-up at the electrode–electrolyte interface. The low-frequency conductivity is decreased due to this charge carrier deficit [51]. In order to understand the polarization effects governed by ionic motion in the bulk, the low-frequency part of the σ′ is fitted to Eq. 2 [52].

Table 6 AC conductivity for all electrolyte samples from A to K infused with TiO_2 nanofillers at 10^5 Hz for various temperatures

Temperature (T)		AC conductivity at 10^5 Hz (σ/mS cm^{-1})										
T (℃)	T (K)	TiO_2 NFs added gel-polymer electrolyte sample										
		A	B	C	D	E	F	G	H	I	J	K
20	293.15	1.18	1.29	1.37	1.50	1.49	1.61	1.61	1.81	1.61	1.56	1.38
30	303.15	1.34	1.45	1.68	1.76	1.72	1.92	1.92	2.23	1.77	1.77	1.47
40	313.15	1.65	1.77	1.89	2.11	2.05	2.27	2.27	2.51	2.05	1.98	1.59
50	323.15	1.91	2.06	2.11	2.41	2.38	2.58	2.58	3.12	2.31	2.21	1.79
60	333.15	2.13	2.26	2.39	2.69	2.66	2.84	2.84	3.17	2.54	2.44	2.02
70	343.15	2.35	2.45	2.64	2.96	2.93	3.15	3.15	3.41	2.70	2.60	2.32
80	353.15	2.57	2.59	2.91	3.17	3.13	3.39	3.39	3.63	2.85	2.82	2.55

$$\sigma_{(\omega)}\prime = A\omega^n \tag{2}$$

where ω is the angular frequency of the applied AC signal and n is a factor that depends on the polarization.

The imaginary part of the AC conductivity (σ'') for sample H is also frequency-dependent, as depicted in Fig. 4b. All the samples (A to K) show a similar trend, with the peaks growing upward with increasing temperature. The relaxation of interfacial charge transport contributes to the peak value of the σ'' AC conductivity. Typically, the imaginary part, σ'', is due to the capacitive effects of the cell prepared by sandwiching an electrolyte between two stainless steel blocking electrodes.

Dielectric constant (ε)

The polarization between the interfaces and the bulk affects the dielectric characteristics of the electrolyte system. Dielectric polarization of the electrolyte plays a significant role in the relative mobility of the positive and negative charges within the assembled cells. The dielectric response of an electrolyte can be characterized by the relative dielectric constant as a complex quantity made up of real and imaginary parts. There, the real (ε') and imaginary (ε'') parts of the dielectric constant represent the quantity of energy stored in an electrolyte material as polarization and energy loss as a function of the applied electric field [53]. The real and imaginary parts of the dielectric constant can be obtained using Eqs. 3 and 4 [50].

$$\varepsilon\prime = -\frac{Z\varepsilon}{\omega.C_0\left(Z\varepsilon^2 + Z'^2\right)} \tag{3}$$

$$\varepsilon\varepsilon = \frac{Z\prime}{\omega.C_0\left(Z\varepsilon^2 + Z\prime^2\right)} \tag{4}$$

where the real part of the impedance, the imaginary part of the impedance, the angular frequency, and the geometrical capacitance are represented by the symbols Z', Z'', ω, and C_0, respectively.

The variations of the real part of the dielectric constant (ε') with frequency for sample H, plotted for different temperatures from 20 to 80 ℃, are shown in Fig. 4c. All other samples (A to K) exhibit similar behavior. The curve shows a decrease of the dielectric constant with the increase in frequency at constant temperature. This behavior can be attributed to the fact that relaxation (orientation and interfacial) and deformational polarization (electronic and ionic) contribute to the dielectric constant value at low frequencies. The orientation and interfacial polarization are significantly dominant at low frequencies [54].

The frequency dependence of the imaginary part (ε'') of the dielectric constant for sample H is captured in Fig. 4d for a range of temperatures between 20 and 80 ℃. The curves demonstrate a decrease of the ε'' with the increase in the frequency at constant temperature. Furthermore, ε'' increases due to the increase in the temperature at a constant frequency. At higher temperatures, dipoles can quickly orient themselves with the field, leading to an increase in the dielectric constant [50, 55]. Also, the imaginary part of the dielectric constant contributes to the DC conductivity at low temperatures [50].

Polarizing microscopy analysis

PEO is abundantly used in preparing gel-polymer electrolytes due to its favorable physicochemical properties. The single helical structure of PEO results in rapid ionic conduction, but PEO is semi-crystalline at room temperature [56]. The crystallization of the PEO can be controlled by adding TiO_2 nanoparticles, which increases the ionic conductivity of the electrolyte. TiO_2 nanoparticles change the PEO polymer matrix and increase the amorphousity of the electrolyte. This creates free spaces, which improves ionic transport [57].

The polarization microscopic images of the electrolyte series obtained by varying TiO_2 nanofiller percentages from

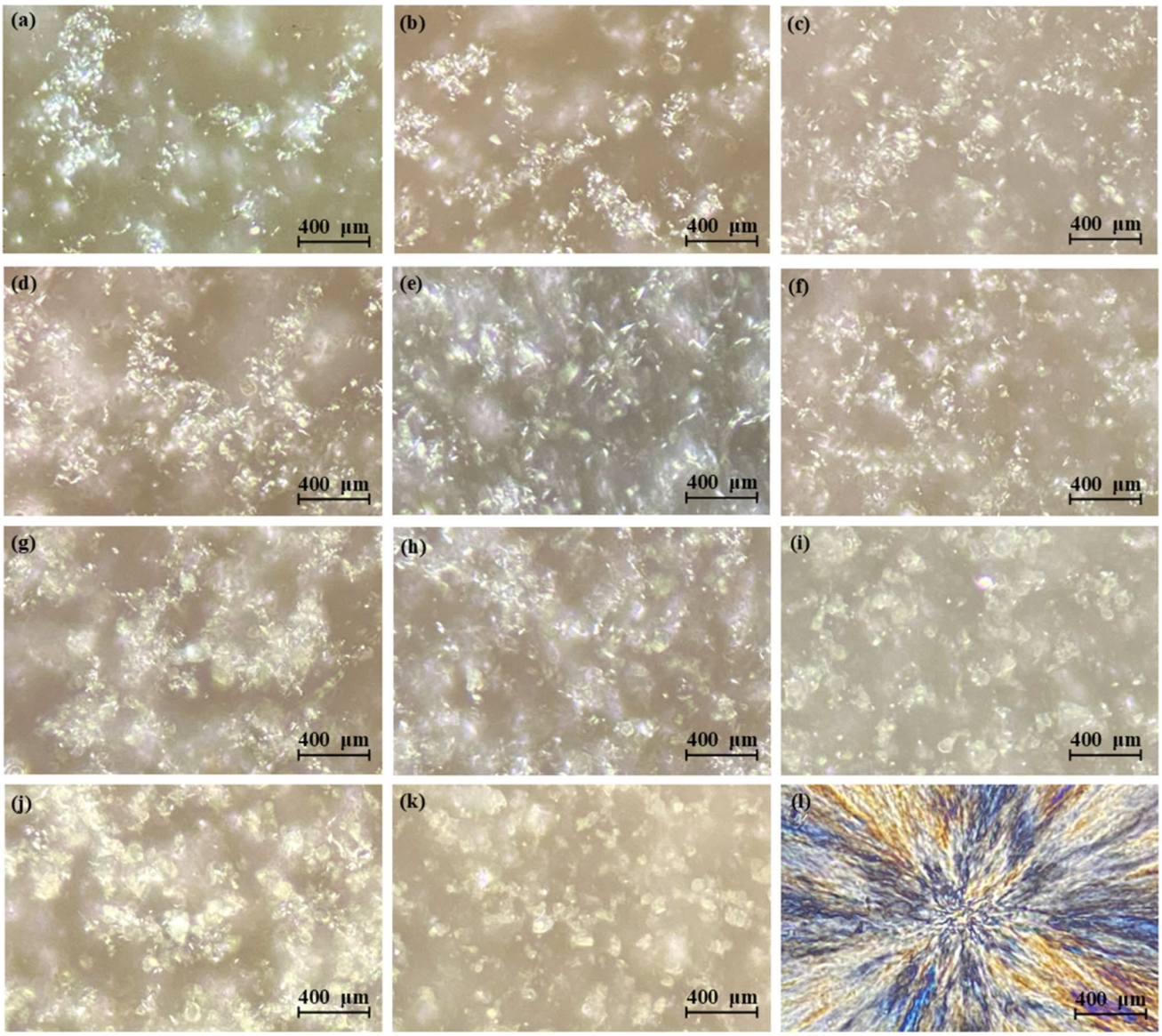

Fig. 5 Polarizing micrographs of **a** sample A, **b** sample B, **c** sample C, **d** sample D, **e** sample E, **f** sample F, **g** sample G, **h** sample H, **i** sample I, **j** sample J, **k** sample K, and **l** pure PEO sample under the magnification × 10 × 40

0 to 25% are shown in Fig. 5a–k. The polarization microscope image of pure PEO polymer is shown in Fig. 5l for comparison. The spherulites formed by lamella structures visible in pure PEO samples are not visible in the electrolyte samples [58, 59]. The microscopic images show the improvement of the amorphousity of the polymer matrix with increasing NF infusion, as well as a uniform distribution of the AFs within the matrix.

DC polarization analysis

For DC polarization measurements, gel-polymer electrolytes were sandwiched between the two stainless steel blocking electrodes with a 0.64 cm^2 hole area with 1 mm thickness. These stainless steel blocking electrodes are suitable for determining the transference number of electrons and ions because only electrons can be passed through these electrodes. The ratio of the measured polarization current to maximum polarization current versus time for the electrolyte series is shown in Fig. 6. The measurements were taken continuously for 30 min. The transference number of ions and electrons was obtained from the graph using Eqs. 5–7.

$$T_e = \frac{I_s}{I_0} \tag{5}$$

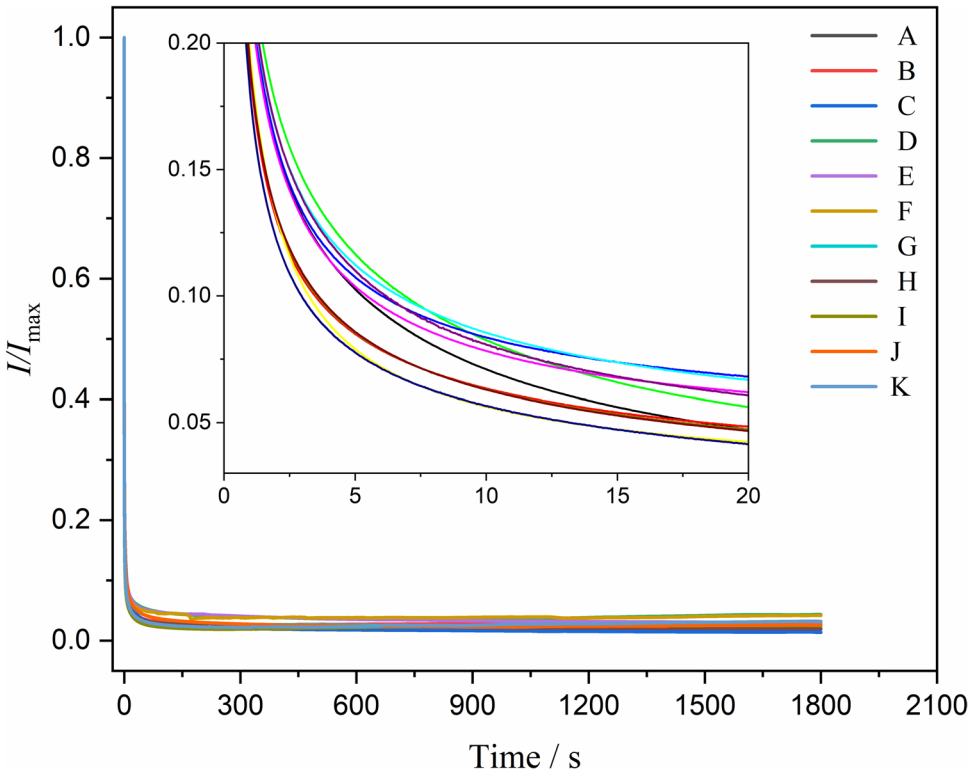

Fig. 6 DC polarization curves of all electrolyte series with varying TiO_2 percentages from 0 to 25%

$$T_{\text{ion}} = \frac{I_0 - I_s}{I_0} \tag{6}$$

$$T_e = 1 - T_{\text{ion}} \tag{7}$$

where the ionic transference number, electronic transference number, initial current, and stable current of polarization are represented by the symbols T_{ion}, T_e, I_0, and I_s, respectively.

When the migration of ions reaches equilibrium, the current approaches the steady state. Within the gel-polymer electrolyte, ions act as dominant charge carriers. Because of that, a drastic drop in the current can be seen in the graphs before reaching the steady-state current. If, instead, the electrons were the dominant charge carrier, this drastic current drop of the current would not be visible. It is possible to conclude that the gel-polymer electrolytes under study consist of ionic charge carriers by using the saturated levels of polarization current [60, 61]. Since the normalized currents were plotted in Fig. 6, the plateau values were used to determine the electronic transference number (I_s/I_o). Based on the plateau of graphs in Fig. 6, all electrolyte samples exhibit ionic transference numbers ranging from 0.96 to 0.99. This indicates that ions play a significant role in conductivity, further confirming that all electrolyte samples are effective ionic conductors.

FTIR spectra and UV–Vis spectra analysis

A set of FTIR spectra for the electrolyte series is shown in Fig. 7a, with the wavenumber scanned from 500 to 3000 cm^{-1}. It indicates the vibration frequencies of molecular bonds associated with EC and PC organic solvents in each electrolyte sample. The FTIR spectra demonstrate the in-plane ring stretching, asymmetric ring stretching, and C–O stretching frequencies at 714.50 cm^{-1}, 1069.34 cm^{-1}, and 1770.33 cm^{-1}, respectively. The vibration frequencies corresponding to the out-of-plane ring bending, C–H wagging, and C–H rocking appear at 772.35 cm^{-1}, 1158.04 cm^{-1}, and 1388.49 cm^{-1}, respectively [62]. Peaks corresponding to additional vibration frequencies are not visible in this FTIR spectra. The data further confirms that the electrolyte is suitable for DSSCs and that there are not any undesired chemical components or byproducts within the electrolytes.

The UV–Vis spectra of the electrolyte series with TiO_2 concentrations ranging from 0 to 25% are shown in Fig. 7b. The absorption edge of the TiO_2 nanoparticles is close to 400 nm, and light absorption by the electrolyte increases with an increase in TiO_2 concentrations, as shown in Fig. 7b. This increase in absorption indicates improved light harvesting, which contributes to higher charge generation and supports dye regeneration. However, high TiO_2 concentration may block the light and impact the electrolyte's transparency, potentially limiting overall efficiency. Therefore,

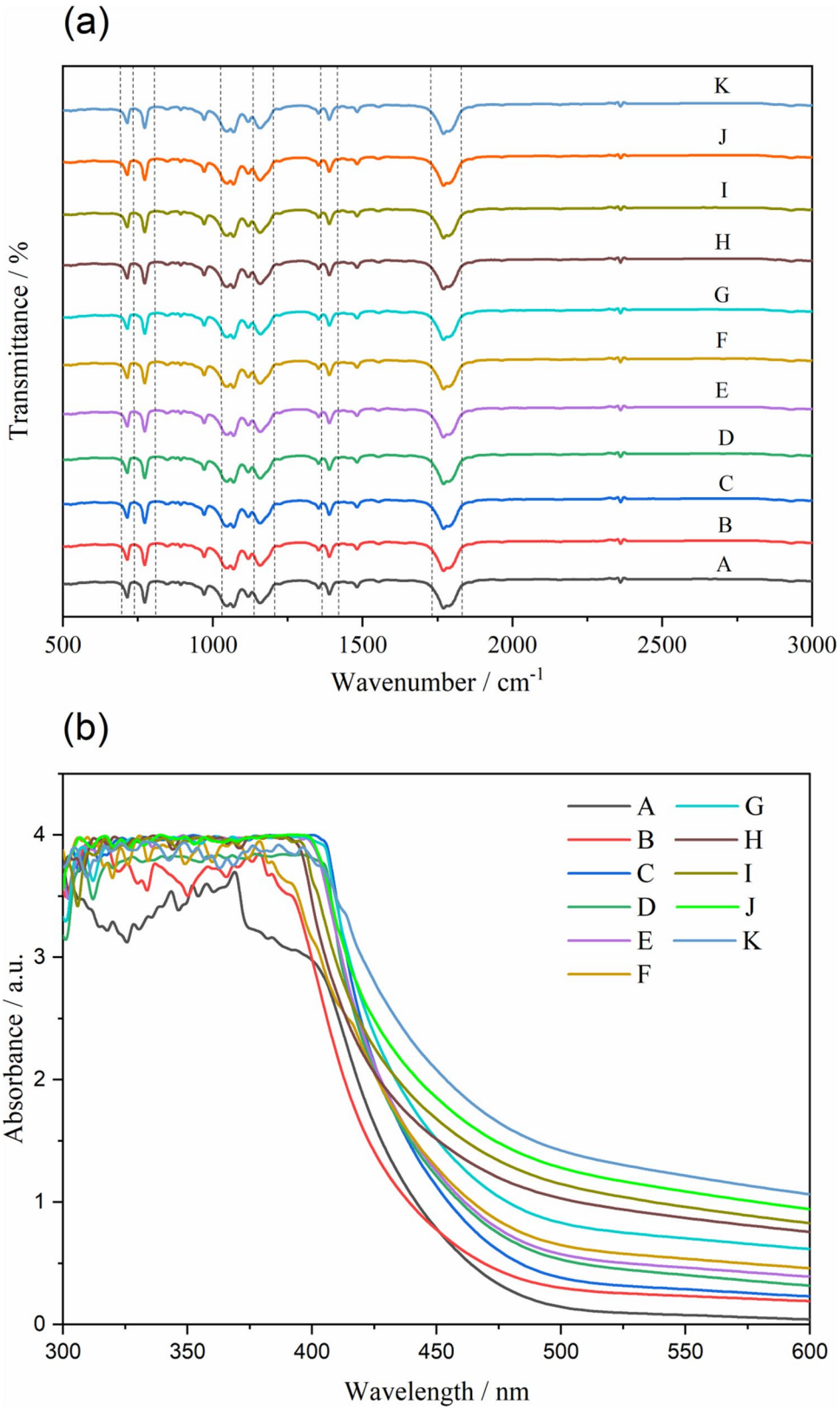

Fig. 7 **a** FTIR spectra recorded from 500 to 3000 cm^{-1} for the electrolyte series with TiO_2 percentages varying from 0 to 25%, **b** UV–Vis absorption spectrum of the electrolyte series with TiO_2 percentages varying from 0 to 25%

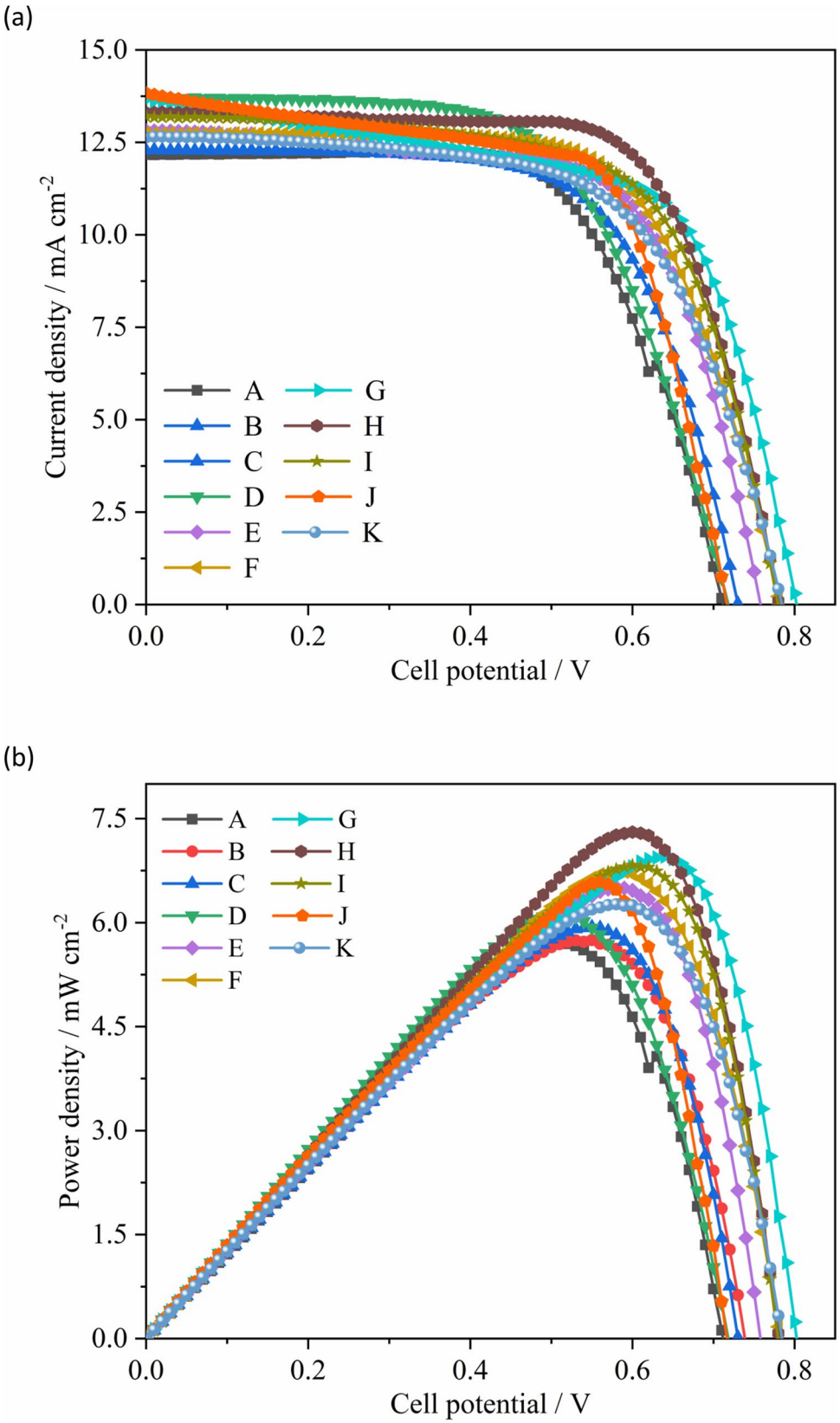

Fig. 8 The variation of **a** current density and **b** power density against cell potential for the DSSCs prepared with the electrolyte series

a TiO_2 concentration of 17.5% is identified as optimal for electrolyte incorporation, considering light absorption, electrolyte transparency, and charge transport [63].

Characterization of DSSCs

The current density variation with the cell potential of DSSCs assembled using the above-analyzed series of electrolytes having various mass percentages of TiO_2 nanoparticles is shown in Fig. 8a. Such curves were used to calculate the open circuit voltage (V_{oc}), short circuit current density (J_{sc}), power conversion efficiency (PCE), and fill factor (FF) of the cells. The fill factor and PCE of the cells were determined using Eqs. 8 and 9.

$$\mathrm{FF} = \frac{\left(V_{\mathrm{opt}} \times J_{\mathrm{opt}}\right)}{\left(V_{\mathrm{oc}} \times J_{\mathrm{sc}}\right)} \tag{8}$$

$$\mathrm{PCE} = \frac{\left(V_{\mathrm{opt}} \times J_{\mathrm{opt}} \times \mathrm{FF}\right)}{\text{total incident power}} \times 100\% \tag{9}$$

In general, the charge transport process of a DSSC depends highly on the conductivity of its electrolyte. The resistance of the electrolyte is a major contribution to the overall resistance of the DSSC devices, and it depends on the electrolyte's conductivity. The short circuit current density and the photocurrent of a DSSC are controlled by the conductivity of the electrolyte.

In this study, the highest photoconversion efficiency was delivered by the DSSCs with the high-conducting electrolyte (sample H) containing 17.50 wt.% TiO_2 NFs. There, the J_{sc}, V_{oc}, and, FF values were 13.30 mA cm^{-2}, 0.78 V, and, 0.70, respectively, for this DSSC. The photoelectrochemical parameters of the DSSC test cell series are listed in Table 7. Here, the high-conducting electrolyte facilitates rapid electron transfer to the dye, which accelerates dye regeneration and increases the V_{oc}. The result in a lower shunt resistance of the cell may contributed to enhancing both the FF and J_{sc}. The variations of power density with the cell potential of the DSSCs for the electrolyte series are shown in Fig. 8b.

An optimal concentration of TiO_2 nanoparticles (17.5%) enhances ionic conductivity and improves charge transport, resulting in higher J_{sc}. At this TiO_2 concentration, charge separation is enhanced, and recombination losses are reduced, leading to a higher V_{oc}. Additionally, the FF represents the quality of the DSSCs, which improves by enhancing charge extraction efficiency and minimizing recombination losses. This optimal concentration also enhances light absorption, charge generation, and transport, resulting in higher power conversion efficiency. However, at higher TiO_2 concentrations, agglomeration may occur, reducing the effective surface area available for charge generation and transport, which affects both J_{sc} and V_{oc}. Additionally, this agglomeration can negatively impact the FF [64].

The variation of energy conversion efficiencies in the DSSCs assembled using the electrolyte series is shown in Fig. 9. The room temperature ionic conductivity variation in the electrolyte is also included in Fig. 9 for the comparison of the conductivity in electrolyte and efficiency in cells. Each cell measured in this study shows efficiencies above 5%. The prototype DSSC assembled with the highest conducting electrolyte (sample H; containing nano-TiO_2 17.50 wt.%) yields the highest efficiency of 7.30%. Consequently, there is a 28.1% power enhancement compared to the efficiency of the reference DSSC assembled with a standard gel-polymer electrolyte (5.70%). The gel-polymer electrolytes under investigation do not contain any volatile solvents like ethanol, acetone, or methanol. In this study, the fabricated DSSCs are stable and environmentally friendly, with a high photoconversion efficiency of up to 7.30%. Compared to the values given in Table 2, the present study reports the highest efficiency for PEO-based TiO_2 nanofiller-integrated DSSCs.

Table 7 Photoelectrochemical parameters of DSSC test cell series

Sample name	J_{sc} (mA cm^{-2})	V_{oc} (V)	FF	PCE (%)
A	12.17	0.71	0.66	5.70
B	12.68	0.74	0.61	5.75
C	12.28	0.73	0.66	5.94
D	13.07	0.72	0.62	6.12
E	11.51	0.76	0.74	6.51
F	12.74	0.80	0.67	6.73
G	13.67	0.80	0.64	6.95
H	13.30	0.78	0.70	7.30
I	13.20	0.78	0.66	6.83
J	13.83	0.72	0.66	6.58
K	12.64	0.78	0.58	6.26

Charge recombination of DSSCs

In order to understand the charge transport and transfer dynamics, electrochemical impedance spectroscopy (EIS) of the DSSCs was analyzed. Bode phase diagrams shown in Fig. 10a were used to calculate the electron transport lifetimes (τ_{tra}) and recombination lifetimes (τ_{rec}) [42, 65]. The DSSCs with the highest conducting electrolyte (sample H) show an electron recombination lifetime of 254.75 ms and a transport lifetime of 65 µs, as per the τ_{rec} and τ_{tra} of DSSCs with filler-free gel-polymer electrolyte, which is 82.47 ms and 44 µs, respectively.

The Nyquist plot of the DSSCs (from EIS analysis) is shown in Fig. 10b. The electron diffusion length (the distance an electron can travel through a material before

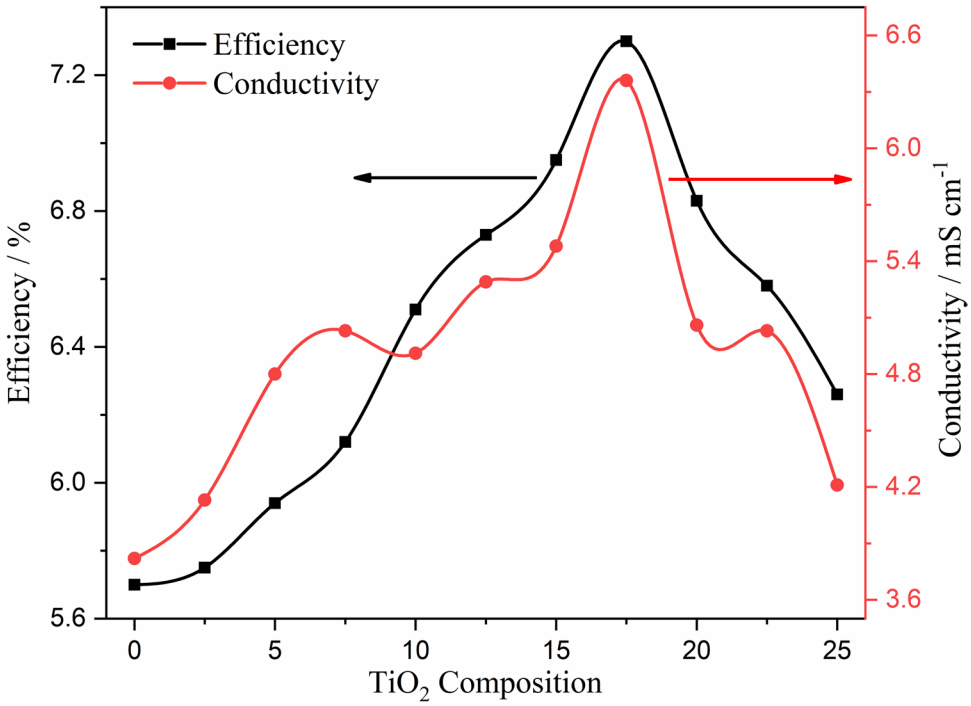

Fig. 9 Variation of the energy conversion efficiency in DSSCs assembled with TiO_2 nanofiller-infused electrolytes and the ionic conductivity in electrolytes

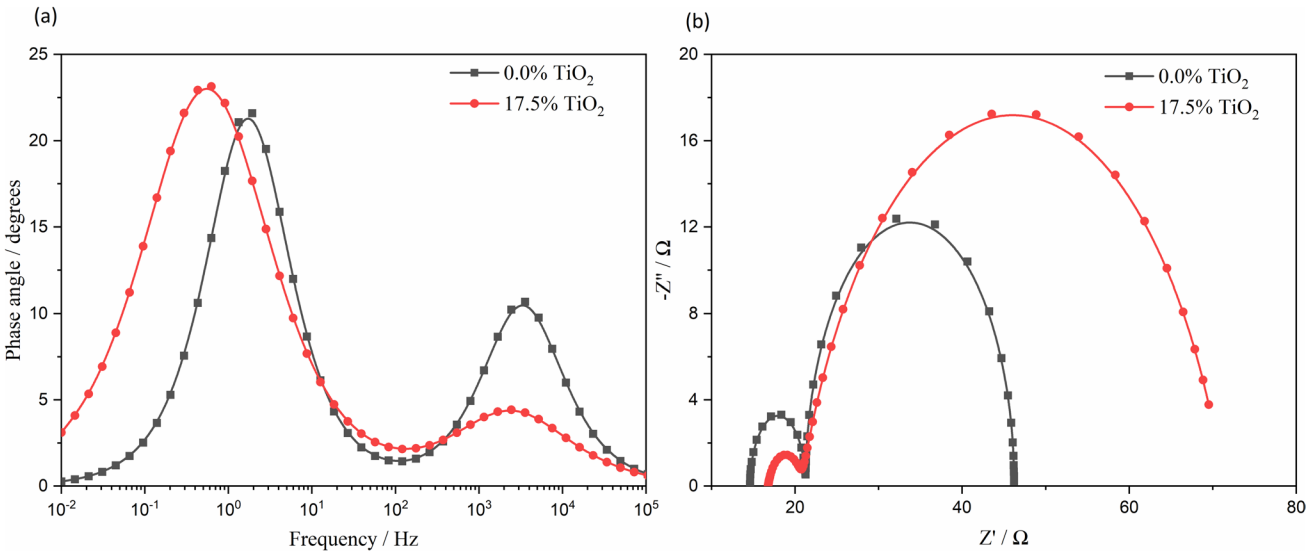

Fig. 10 **a** The bode phase diagrams and **b** Nyquist plot of the DSSCs containing the highest conducting electrolyte (17.5% TiO_2) and filler-free gel-polymer electrolyte

recombining with photogenerated a hole) was obtained from the graph using Eq. 10

$$D_L = L\sqrt{\frac{R_{rec}}{R_{tra}}} \tag{10}$$

where the diffusion length, thickness of the TiO_2 layer of photoanode, recombination resistance, and transfer resistance are represented by the symbols D_L, L, R_{rec}, and R_{tra}, respectively. The R_{rec} and R_{tra} were obtained from the Nyquist plot. The diameter of the low-frequency semicircle is attributed to the R_{rec} and that of the high-frequency semicircle is attributed to the R_{tra}. $L = 5.2$ nm was determined by analyzing correctional SEMs given in Fig. 11b. The infusion of TiO_2 NFs into the electrolyte reduced the photoelectron recombination resistance at the interface between the TiO_2 photoanode and electrolyte. Therefore, most of the generated photoelectrons diffuse through the TiO_2 layers before

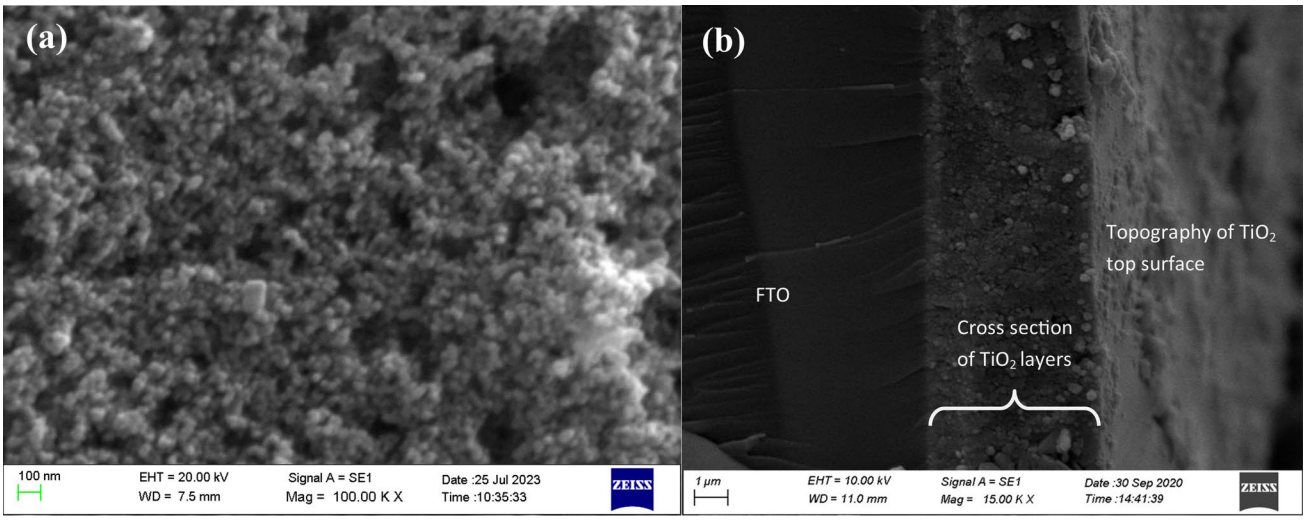

Fig. 11 **a** Surface SEM image of 6-layer photoanodes at 100 K magnification, **b** labeled cross-sectional SEM images of 6-layer photoanode at 15 K magnification

recombination, resulting in an increased average diffusion length [66]. The diffusion lengths of the DSSCs with the highest conducting electrolyte and the filler-free gel-polymer electrolyte are 16.09 µm and 9.86 µm, respectively. The higher efficiency given with filler-added electrolyte (TiO_2 17.50 wt.%) can be attributed to the increased electron diffusion length.

The surface morphology of the 6-layer photoanode is shown in Fig. 11a, demonstrating a well-formed and uniform film without significant surface defects or visible cracks. This ensures effective dye adsorption and optimal light absorption. The absence of cracks indicates a mechanically stable film, resulting in efficient electron transport within the TiO_2 layers. Additionally, effective dye adsorption enhances photocurrent generation by providing a larger surface area for dye molecules to bind [67, 68]. These morphological properties enhance light-harvesting efficiency and contribute to the overall improvement in the PCE of all the DSSCs, given that similar photoanodes are employed throughout this study. However, the electron diffusion length (D_L) varies depending on the electrolyte used. Figure 11b presents the cross-sectional image of the 6-layer photoanode, revealing an approximately uniform thickness of 5.2 µm. This thickness was utilized to calculate D_L for cells incorporating different electrolytes. This uniform deposition facilitates the maintenance of electron transport pathways and enhances the overall PCE of the cell.

Conclusions

The presented study is on the gel-polymer electrolyte modified by infusing nanofillers (NFs), which is suitable for fabricating environmentally friendly and stable dye-sensitized solar cell DSSCs with high energy conversion efficiency. NFs used here are TiO_2 nanoparticles. The ionic conductivity of the electrolytes initially increases with an increase in TiO_2 content up to 17.5% TiO_2 and then decreases with any further increase in TiO_2 percentage. The optimum TiO_2 content in the electrolyte is 17.5%, for both conductivity and DSSC performance. Also, the temperature-dependent ionic conductivity of the electrolyte series showed non-Arrhenius behavior. The maximum conductivity values reported for all the temperatures from 20 to 80 ℃ were given by the electrolyte sample infused with 17.5 wt.% of TiO_2 NFs (sample H). Those conductivity values are 5.18, 6.36, 7.18, 8.06, 8.95, 9.77, and 10.43 mS cm^{-1} at 20 ℃, 30 ℃, 40 ℃, 50 ℃, 60 ℃, 70 ℃, and 80 ℃, respectively. The frequency-dependent electrical and dielectric characteristics of electrolytes were analyzed in terms of real and imaginary parts of the AC conductivity. The real part of the AC conductivity exponentially decreases with the decrease as well as with the decrease in temperature; the imaginary parts of the AC conductivity peak between 1 and 10 kHz.

The development of the amorphousity of the polymer network with the increase in NF amount is evident from the polarization micrographs, which result in improving the conductivity of the electrolyte. DC polarization analysis reveals that the ionic transference number of all electrolyte samples is greater than 0.96. This signifies a higher ionic contribution to the conductivity, inferring that the nano-infused electrolytes under study can be considered efficient electrolytes.

In order to further characterize the performance of the nano-modified electrolytes, DSSCs were assembled using commercial N719 sensitizer dye, TiO_2-based photoanodes, and standard platinum counter electrodes. Every cell showed efficiency above 5%. The DSSCs assembled

with the electrolyte sample containing the optimal amount (17.5 wt.%) of TiO_2 NFs yielded a maximum efficiency of 7.30%, resulting in a 28.1% power enhancement compared to DSSCs assembled with standard gel-polymer electrolyte. Based on the EIS analysis of DSSCs, the recombination lifetimes and diffusion length of the DSSCs with high-conducting electrolyte sample (17.5% TiO_2) are higher due to the reduced recombination resistance at the interface between photoanode and electrolyte, caused by the incorporation of TiO_2 NFs into the electrolyte. Those τ_{rec} and D_L values are 254.75 ms and 16.09 µm, respectively. Therefore, this study provides valuable insights into the potential role of nanofiller-infused gel-polymer electrolytes in developing high-performance DSSCs that are non-toxic, stable, and efficient.

Supplementary Information The online version contains supplementary material available at https://doi.org/10.1007/s10008-024-06169-x.

Acknowledgements Technical assistance from Dr. E.M.S.G.M. Edirisooriya, Department of Geology, and Mr. C.U. Wadasinghe, Department of Physics, University of Peradeniya, Sri Lanka, is gratefully acknowledged.

Funding The study is funded by Post-graduate Institute of Science, University of Peradeniya, Sri Lanka, Research Grant No. PGIS/2022/12 and University of Peradeniya, Sri Lanka, Grant No. PGIS/2023/34/S.

References

1. Green M, Dunlop E, Hohl-Ebinger J, Yoshita M, Kopidakis N, Hao X (2021) Solar cell efficiency tables (version 57). Prog Photovoltaics Res Appl 29(1):3–15
2. Saga T (2010) Advances in crystalline silicon solar cell technology for industrial mass production. npg Asia Mater 2(3):96–102
3. Jena A, Mohanty SP, Kumar P, Naduvath J, Gondane V, Lekha P, Bhargava P (2012) Dye sensitized solar cells: a review. Trans Indian Ceram Soc 71(1):1–16
4. Bandara TMWJ, Jayasundara WJMJSR, Fernado HDNS, Dissanayake MAKL, De Silva LAA, Albinsson I, Furlani M, Mellander BE (2015) Efficiency of 10% for quasi-solid state dye-sensitized solar cells under low light irradiance. J Appl Electrochem 45:289–298
5. Sharma K, Sharma SS, Ray J, Chaure NB (2023) Investigation of Ru-complex free natural dye for the application of dye sensitized solar cells. J Integrated Sci Technol 11(3):529–529
6. Grätzel M (2005) Solar energy conversion by dye-sensitized photovoltaic cells. Inorg Chem 44(20):6841–6851
7. Hagfeldt A, Boschloo G, Sun L, Kloo L, Pettersson H (2010) Dye-sensitized solar cells. Chem Rev 110(11):6595–6663
8. Wu J, Lan Z, Hao S, Li P, Lin J, Huang M, ... & Huang Y (2008) Progress on the electrolytes for dye-sensitized solar cells. Pure Appl Chem 80(11):2241–2258.
9. Wu J, Lan Z, Lin J, Huang M, Huang Y, Fan L, Luo G (2015) Electrolytes in dye-sensitized solar cells. Chem Rev 115(5):2136–2173
10. Bella F, Gerbaldi C, Barolo C, Grätzel M (2015) Aqueous dye-sensitized solar cells. Chem Soc Rev 44(11):3431–3473
11. Farhana NK, Saidi NM, Bashir S, Ramesh S, Ramesh K (2021) Review on the revolution of polymer electrolytes for dye-sensitized solar cells. Energy Fuels 35(23):19320–19350
12. Venkatesan S, Lee YL (2017) Nanofillers in the electrolytes of dye-sensitized solar cells–a short review. Coord Chem Rev 353:58–112
13. Bella F, Ozzello ED, Sacco A, Bianco S, Bongiovanni R (2014) Polymer electrolytes for dye-sensitized solar cells prepared by photopolymerization of PEG-based oligomers. Int J Hydrogen Energy 39(6):3036–3045
14. Ren Y, Zhang D, Suo J, Cao Y, Eickemeyer FT, Vlachopoulos N, ... & Grätzel M (2023) Hydroxamic acid pre-adsorption raises the efficiency of cosensitized solar cells. Nature, 613(7942):60–65.
15. Ebenezer Anitha A, Dotter M (2023) A review on liquid electrolyte stability issues for commercialization of dye-sensitized solar cells (DSSC). Energies 16(13):5129
16. Teo LP, Buraidah MH, Arof AK (2020) Polyacrylonitrile-based gel polymer electrolytes for dye-sensitized solar cells: a review. Ionics 26(9):4215–4238
17. Hasan MM, Islam MD, Rashid TU (2020) Biopolymer-based electrolytes for dye-sensitized solar cells: a critical review. Energy Fuels 34(12):15634–15671
18. Bella F, Sacco A, Massaglia G, Chiodoni A, Pirri CF, Quaglio M (2015) Dispelling clichés at the nanoscale: the true effect of polymer electrolytes on the performance of dye-sensitized solar cells. Nanoscale 7(28):12010–12017
19. Bella F, Bongiovanni R (2013) Photoinduced polymerization: an innovative, powerful and environmentally friendly technique for the preparation of polymer electrolytes for dye-sensitized solar cells. J Photochem Photobiol, C 16:1–21
20. Pitawala HMJC, Dissanayake MAKL, Seneviratne VA (2007) Combined effect of Al2O3 nano-fillers and EC plasticizer on ionic conductivity enhancement in the solid polymer electrolyte (PEO) 9LiTf. Solid State Ionics 178(13–14):885–888
21. Pitawala HMJC, Dissanayake MAKL, Seneviratne VA, Mellander BE, Albinson I (2008) Effect of plasticizers (EC or PC) on the ionic conductivity and thermal properties of the (PEO) 9 LiTf: Al2O3 nanocomposite polymer electrolyte system. J Solid State Electrochem 12:783–789
22. Venkatesan S, Liu IP, Chen LT, Hou YC, Li CW, Lee YL (2016) Effects of TiO2 and TiC nanofillers on the performance of dye sensitized solar cells based on the polymer gel electrolyte of a cobalt redox system. ACS Appl Mater Interfaces 8(37):24559–24566
23. Venkatesan S, Surya Darlim E, Tsai MH, Teng H, Lee YL (2018) Graphene oxide sponge as nanofillers in printable electrolytes in high-performance quasi-solid-state dye-sensitized solar cells. ACS Appl Mater Interfaces 10(13):10955–10964
24. Chang WC, Sie SY, Yu WC, Lin LY, Yu YJ (2016) Preparation of nano-composite gel electrolytes with metal oxide additives for dye-sensitized solar cells. Electrochim Acta 212:333–342
25. Sebo B, Huang N, Liu Y, Tai Q, Liang L, Hu H, ... & Zhao XZ (2013) Dye-sensitized solar cells enhanced by optical absorption, mediated by TiO2 nanofibers and plasmonics Ag nanoparticles. Electrochimica Acta 112:458–464.
26. Diebold U (2003) Structure and properties of TiO2 surfaces: a brief review. Appl Phys A 76:681–687
27. Djerdj I, Tonejc AM (2006) Structural investigations of nanocrystalline TiO2 samples. J Alloy Compd 413(1–2):159–174
28. Dastan D, Chaure N, Kartha M (2017) Surfactants assisted solvothermal derived titania nanoparticles: synthesis and simulation. J Mater Sci: Mater Electron 28:7784–7796
29. Dissanayake MAKL, Rupasinghe WNS, Seneviratne VA, Thotawatthage CA, Senadeera GKR (2024) Efficiency enhancement due to the combined mixed cation effect and TiO2 nanofiller effect in PEO and ionic liquid-based dye-sensitized solar cells. J Solid State Electrochem 28:2561–2571
30. Dissanayake MAKL, Jaseetharan T, Senadeera GKR, Mellander BE, Albinsson I, Furlani M, Kumari JMKW (2021) Solid-state solar cells co-sensitized with PbS/CdS quantum dots and N719

dye and based on solid polymer electrolyte with binary cations and nanofillers. J Photochem Photobiol, A 405:112915
31. Lim SM, Moon J, Baek UC, Lee JY, Chae Y, Park JT (2021) Shape-controlled TiO2 nanomaterials-based hybrid solid-state electrolytes for solar energy conversion with a mesoporous carbon electrocatalyst. Nanomaterials 11(4):913
32. Chawarambwa FL, Putri TE, Attri P, Kamataki K, Itagaki N, Koga K, Shiratani M (2021) Effects of concentrated light on the performance and stability of a quasi-solid electrolyte in dye-sensitized solar cells. Chem Phys Lett 781:138986
33. Vinoth S, Kanimozhi G, Kumar H, Srinadhu ES, Satyanarayana N (2019) High conducting nanocomposite electrospun PVDF-HFP/TiO2 TiO2 quasi-solid electrolyte for dye-sensitized solar cell. J Mater Sci: Mater Electron 30:1199–1213
34. Liu IP, Wang LW, Tsai MH, Chen YY, Teng H, Lee YL (2019) A new mechanism for interpreting the effect of TiO2 nanofillers in quasi-solid-state dye-sensitized solar cells. J Power Sources 433:226693
35. Dissanayake MAKL, Rupasinghe WNS, Seneviratne VA, Thotawatthage CA, Senadeera GKR (2014) Optimization of iodide ion conductivity and nano filler effect for efficiency enhancement in polyethylene oxide (PEO) based dye sensitized solar cells. Electrochim Acta 145:319–326
36. Trang TT, Lee DK, Kim JH (2013) Enhancing the ionic transport of PEO-based composite polymer electrolyte by addition of TiO2 nanofiller for quasi-solid state dye-sensitized solar cells. Met Mater Int 19:1369–1372
37. Sivakumar R, Akila K, Anandan S (2010) New type of inorganic–organic hybrid (heteropolytungsticacid–polyepichlorohydrin) polymer electrolyte with TiO2 nanofiller for solid state dye sensitized solar cells. Curr Appl Phys 10(5):1255–1260
38. Anandan S (2008) Viologen impregnated PVDF with TiO2 nanofiller as a solid polymer electrolyte for dye-sensitized solar cells. Curr Appl Phys 8(1):99–103
39. Kang MS, Ahn KS, Lee JW (2008) Quasi-solid-state dye-sensitized solar cells employing ternary component polymer-gel electrolytes. J Power Sources 180(2):896–901
40. Nishshanke GBMMM, Arof AK, Bandara TMWJ (2020) Review on mixed cation effect in gel polymer electrolytes for quasi solid-state dye-sensitized solar cells. Ionics 26:3685–3704
41. Nishshanke GBMMM, Thilakarathna BDKK, Albinsson I, Mellander BE, Bandara TMWJ (2021) Multi-layers of TiO2 nanoparticles in the photoelectrode and binary iodides in the gel polymer electrolyte based on poly (ethylene oxide) to improve quasi solid-state dye-sensitized solar cells. J Solid State Electrochem 25:707–720
42. Bandara TMWJ, Gunathilake SMS, Nishshanke GBMMM, Dissanayake MAKL, Chaure NB, Olusola OI, Mellander B-E, Furlani M, Albinsson I (2023) Efficiency enhancement and chrono-photoelectron generation in dye-sensitized solar cells based on spin-coated TiO2 nanoparticle multilayer photoanodes and a ternary iodide gel polymer electrolyte. J Mater Sci: Mater Electron 34(28):1969
43. Arof AK, Aziz MF, Noor MM, Careem MA, Bandara LRAK, Thotawatthage CA, Rupasinghe WNS, Dissanayake MAKL (2014) Efficiency enhancement by mixed cation effect in dye-sensitized solar cells with a PVDF based gel polymer electrolyte. Int J Hydrogen Energy 39(6):2929–2935
44. Bandara TMWJ, Mellander BE, Albinsson I, Dissanayake MAKL (2009) Effect of thermal history and characterization of plasticized, composite polymer electrolyte based on PEO and tetrapropylammonium iodide salt (Pr4N+ I-). Solid State Ionics 180(4–5):362–367
45. Marcinek M, Bac A, Lipka P, Zalewska A, Żukowska G, Borkowska R, Wieczorek W (2000) Effect of filler surface group on ionic interactions in PEG− LiClO4− Al2O3 composite polyether electrolytes. J Phys Chem B 104(47):11088–11093
46. Jayathilaka PARD, Dissanayake MAKL, Albinsson I, Mellander BE (2002) Effect of nano-porous Al2O3 on thermal, dielectric and transport properties of the (PEO) 9LiTFSI polymer electrolyte system. Electrochim Acta 47(20):3257–3268
47. Abdukarimov A, Noor ISM, Mamatkarimov O, Arof AKM (2022) Influence of charge carrier density, mobility and diffusivity on conductivity–temperature dependence in polyethylene oxide–based gel polymer electrolytes. High Perform Polym 34(2):232–241
48. Abdul Aziz NA, Tarmizi EZM, Razak CSC, Noor IM (2022) Impact of charge carrier transport properties on conductivity-temperature dependence of gellan gum-LiCF3SO3 biopolymer electrolyte. High Perform Polym 34(6):691–700
49. Bandara TMWJ, Senavirathna SLN, Wickramasinghe HMN, Vignarooban K, De Silva LA, Dissanayake MAKL, ... & Mellander BE (2020) Binary counter ion effects and dielectric behavior of iodide ion conducting gel-polymer electrolytes for high-efficiency quasi-solid-state solar cells. Physical Chemistry Chemical Physics, 22(22):12532–12543.
50. Dhatarwal P, Sengwa RJ (2020) Dielectric polarization and relaxation processes of the lithium-ion conducting PEO/PVDF blend matrix-based electrolytes: effect of TiO2 nanofiller. SN Appl Sci 2(5):833
51. Shukla N, Thakur AK, Shukla A, Marx DT (2014) Ion conduction mechanism in solid polymer electrolyte: an applicability of almond-west formalism. Int J Electrochem Sci 9(12):7644–7659
52. Hanefeld M, Gruszka P, Huth M (2021) AC conductivity and correlation effects in nano-granular Pt/C. Sci Rep 11(1):15163
53. Chérif SF, Chérif A, Dridi W, Zid MF (2020) Ac conductivity, electric modulus analysis, dielectric behavior and bond valence sum analysis of Na3Nb4As3O19 compound. Arab J Chem 13(6):5627–5638
54. Feng Y, Wang CH, Liu SX (2016) Low dielectric constant of polymer based composites induced by the restricted polarizability in the interface. Mater Lett 185:491–494
55. Abdukarimov A, Shah S, Teo LP, Buraidah MH, Abidin ZHZ, Mamatkarimov OO, Arof AK (2020) Characteristics of dye-sensitized solar cells (DSSCs) using liquid and gel polymer electrolytes with tetrapropylammonium salt. Opt Quant Electron 52:1–15
56. Chen XC, Sacci RL, Osti NC, Tyagi M, Wang Y, Keum JK, Dudney NJ (2021) Study of the segmental dynamics and ion transport of solid polymer electrolytes in the semi-crystalline state. Front Chem 8:592604
57. Poonam S, Dinesh Kumar K & Nirali G (2012) Effect of nanofiller on structural and ionic transport properties of plasticized polymer electrolyte. Open J Organic Polym Mater 2012.
58. Marzantowicz M, Dygas JR, Krok F, Nowiński JL, Tomaszewska A, Florjańczyk Z, Zygadło-Monikowska E (2006) Crystalline phases, morphology and conductivity of PEO: LiTFSI electrolytes in the eutectic region. J Power Sources 159(1):420–430
59. Aziz SB, Nofal MM, Brza MA, Hussein SA, Mahmoud KH, El-Bahy ZM, ... & Hussein AM (2021) Characteristics of PEO incorporated with CaTiO3 nanoparticles: structural and optical properties. Polymers 13(20):3484.
60. Saidi NM, Farhana NK, Ramesh S, Ramesh K (2021) Influence of different concentrations of 4-tert-butyl-pyridine in a gel polymer electrolyte towards improved performance of dye-sensitized solar cells (DSSC). Sol Energy 216:111–119
61. Buraidah MH, Shah S, Teo LP, Chowdhury FI, Careem MA, Albinsson I, ... & Arof AK (2017) High efficient dye sensitized solar cells using phthaloylchitosan based gel polymer electrolytes. Electrochimica Acta 245:846–853.
62. Saidi NM, Omar FS, Numan A, Apperley DC, Algaradah MM, Kasi R, ... & Subramaniam RT (2019) Enhancing the efficiency

of a dye-sensitized solar cell based on a metal oxide nanocomposite gel polymer electrolyte. ACS Appl Mater Interfaces 11(33):30185–30196.
63. Govindaraj R, Pandian MS, Ramasamy P, Mukhopadhyay S (2015) Sol–gel synthesized mesoporous anatase titanium dioxide nanoparticles for dye sensitized solar cell (DSSC) applications. Bull Mater Sci 38:291–296
64. Xi J, Zhang Q, Park K, Sun Y, Cao G (2011) Enhanced power conversion efficiency in dye-sensitized solar cells with TiO2 aggregates/nanocrystallites mixed photoelectrodes. Electrochim Acta 56(5):1960–1966
65. Bisquert J, Mora-Sero I (2010) Simulation of steady-state characteristics of dye-sensitized solar cells and the interpretation of the diffusion length. The Journal of Physical Chemistry Letters 1(1):450–456
66. Chen CL, Teng H, Lee YL (2011) In situ gelation of electrolytes for highly efficient gel-state dye-sensitized solar cells. Adv Mater 23(36):4199–4204
67. Nandi P, Das D (2022) Morphological variations of ZnO nanostructures and its influence on the photovoltaic performance when used as photoanodes in dye sensitized solar cells. Sol Energy Mater Sol Cells 243:111811
68. Hossain MK, Pervez MF, Uddin MJ, Tayyaba S, Mia MNH, Bashar MS, ... & Khan MA (2018) Influence of natural dye adsorption on the structural, morphological and optical properties of TiO2 based photoanode of dye-sensitized solar cell. Mater Sci 36:93–101.

Terms and Conditions

Springer Nature journal content, brought to you courtesy of Springer Nature Customer Service Center GmbH (“Springer Nature”).
Springer Nature supports a reasonable amount of sharing of research papers by authors, subscribers and authorised users (“Users”), for small-scale personal, non-commercial use provided that all copyright, trade and service marks and other proprietary notices are maintained. By accessing, sharing, receiving or otherwise using the Springer Nature journal content you agree to these terms of use (“Terms”). For these purposes, Springer Nature considers academic use (by researchers and students) to be non-commercial.
These Terms are supplementary and will apply in addition to any applicable website terms and conditions, a relevant site licence or a personal subscription. These Terms will prevail over any conflict or ambiguity with regards to the relevant terms, a site licence or a personal subscription (to the extent of the conflict or ambiguity only). For Creative Commons-licensed articles, the terms of the Creative Commons license used will apply.
We collect and use personal data to provide access to the Springer Nature journal content. We may also use these personal data internally within ResearchGate and Springer Nature and as agreed share it, in an anonymised way, for purposes of tracking, analysis and reporting. We will not otherwise disclose your personal data outside the ResearchGate or the Springer Nature group of companies unless we have your permission as detailed in the Privacy Policy.
While Users may use the Springer Nature journal content for small scale, personal non-commercial use, it is important to note that Users may not:

1. use such content for the purpose of providing other users with access on a regular or large scale basis or as a means to circumvent access control;
2. use such content where to do so would be considered a criminal or statutory offence in any jurisdiction, or gives rise to civil liability, or is otherwise unlawful;
3. falsely or misleadingly imply or suggest endorsement, approval , sponsorship, or association unless explicitly agreed to by Springer Nature in writing;
4. use bots or other automated methods to access the content or redirect messages
5. override any security feature or exclusionary protocol; or
6. share the content in order to create substitute for Springer Nature products or services or a systematic database of Springer Nature journal content.

In line with the restriction against commercial use, Springer Nature does not permit the creation of a product or service that creates revenue, royalties, rent or income from our content or its inclusion as part of a paid for service or for other commercial gain. Springer Nature journal content cannot be used for inter-library loans and librarians may not upload Springer Nature journal content on a large scale into their, or any other, institutional repository.
These terms of use are reviewed regularly and may be amended at any time. Springer Nature is not obligated to publish any information or content on this website and may remove it or features or functionality at our sole discretion, at any time with or without notice. Springer Nature may revoke this licence to you at any time and remove access to any copies of the Springer Nature journal content which have been saved.
To the fullest extent permitted by law, Springer Nature makes no warranties, representations or guarantees to Users, either express or implied with respect to the Springer nature journal content and all parties disclaim and waive any implied warranties or warranties imposed by law, including merchantability or fitness for any particular purpose.
Please note that these rights do not automatically extend to content, data or other material published by Springer Nature that may be licensed from third parties.
If you would like to use or distribute our Springer Nature journal content to a wider audience or on a regular basis or in any other manner not expressly permitted by these Terms, please contact Springer Nature at

onlineservice@springernature.com